14th International Symposium on Turbulence and Shear Flow Phenomena (TSFP14)
Heidelberg, Germany, July 28–31, 2026

TIME RESPONSE OF UNSTEADY CHANNEL FLOWS UNDER THE COMBINED EFFECTS OF A PRESSURE GRADIENT AND ROUGHNESS

M. Mauriello
Department of Aeronautics and Astronautics
University of Southampton
Southampton S016 7QF United Kingdom
mariadebora.mauriello@soton.ac.uk

B. Ganapathisubramani
Department of Aeronautics and Astronautics
University of Southampton
Southampton S016 7QF United Kingdom
g.bharath@soton.ac.uk

N. D. Sandham
Department of Aeronautics and Astronautics
University of Southampton
Southampton S016 7QF United Kingdom
n.sandham@soton.ac.uk

ABSTRACT
Direct numerical simulations (DNS) are performed to investigate the temporal response of turbulent channel flows to an abrupt change in the streamwise pressure gradient. The initial conditions correspond to statistically stationary pure Couette and mixed Poiseuille-Couette flows at $Re_\tau = 590$, with both smooth-smooth and rough-smooth wall configurations. A time-dependent control volume approach is used to extract the friction on the rough surface. Results show that wall roughness significantly alters the transient adjustment following the pressure gradient change, relative to smooth-wall cases, leading to a faster evolution towards the final state. In addition, favourable pressure gradient transients are more monotonic overall, whereas adverse pressure gradient cases display an irregular response. The adjustment dynamics is examined in the inner and outer regions. In the logarithmic region, roughness suppresses much of the history dependence. Time histories of the velocity at the inflection point and of the shear stress at the bottom wall are used to capture the general rate of adjustment of the transient flow.

INTRODUCTION
Unsteady flow conditions are frequently encountered in both engineering applications and natural systems, where changes in driving forces such as pressure gradients or wall motion can provoke complex transient responses in turbulent wall-bounded flows. Numerous studies have been conducted on periodic unsteady flows. Scotti and Piomelli (2001) studied how a turbulent channel flow responds when a periodic (pulsating) fluctuating component adds to the pressure gradient, and demonstrated that the response of turbulence to periodic forcing is governed by the ratio between the oscillation frequency and the characteristic relaxation time of the eddies. They identified a frozen turbulence regime at high frequencies, where the turbulent stresses are unable to track the rapid changes in the mean strain rate, leading to a decoupling of the inner and outer layer responses.

Beyond periodic flows, the structural evolution of turbulence during temporal acceleration has been investigated to understand how the flow reaches a new equilibrium. Kharghani and PasandidehFard (2022) studied temporal flow acceleration over a flat plate with non-zero pressure gradient, and demonstrated that under such transients, the suppression of turbulence in favorable pressure gradients (FPG) and its enhancement in adverse pressure gradients (APG) is not a uniform process across all velocity components. Their work highlights a wall-first adjustment mechanism where the near wall region reaches a quasi-steady state faster than the outer flow. The response to a step-change transient was studied by Chung (2005), who identified a distinct two-stage relaxation process: the mean velocity profile responds almost immediately to the new pressure gradient condition, while the turbulent fluctuations, particularly the Reynolds shear stress, exhibit a significant temporal lag. This study demonstrated that the memory of the initial state is maintained longer in the outer region of the flow, as the structural reorganisation of the large-scale eddies is a much slower process than the near-wall viscous adjustment. A related smooth-wall DNS study by He & Seddighi (2013) showed that, following a rapid increase in flow rate, the transient channel flow evolves through distinct pre-transition, transition and fully turbulent stages rather than adjusting monotonically from one equilibrium state to another.

The presence of wall roughness significantly alters these dynamics. Seddighi *et al.* (2011a) observed that unlike smooth-wall cases, where the turbulence reorganisation is delayed, wall roughness acts to accelerate the transition between equilibrium states. Specifically, they found that the enhanced mixing and higher levels of turbulent production near the wall in rough-surface configurations reset the flow more quickly than in smooth-wall equivalents. A more detailed analysis was later provided by Seddighi *et al.* (2015) for a channel with a pyramid-roughened wall, where the boundary layer over the rough wall was shown to develop faster than over a smooth wall, and the near-wall turbulence adjusted much earlier than the core flow. Their results indicated that the transient over the rough wall proceeds through a process resembling roughness-induced transition, involving the formation and breakdown of strong hairpin vortices and streaks, with the direct effect of roughness largely confined to the region close to the wall.

Bottom wall			Top wall			Π		Steady state		Notation
Rough	Smooth	U_B	Rough	Smooth	U_T	Initial	Final	Initial	Final	
	✓	0		✓	+40	0	−1	C_{SS^+}	PC_{SS^+}	$FPG_{SS_{01}}$
	✓	0		✓	+40	−1	0	PC_{SS^+}	C_{SS^+}	$FPG_{SS_{10}}$
✓		0		✓	+40	0	−1	C_{RS^+}	PC_{RS^+}	$FPG_{RS_{01}}$
✓		0		✓	+40	−1	0	PC_{RS^+}	C_{RS^+}	$FPG_{RS_{10}}$
	✓	0		✓	−40	−1	0	PC_{SS^-}	C_{SS^-}	$APG_{SS_{10}}$
✓		0		✓	−40	0	−1	C_{RS^-}	PC_{RS^-}	$APG_{RS_{01}}$
✓		0		✓	−40	−1	0	PC_{RS^-}	C_{RS^-}	$APG_{RS_{10}}$

Table 1: Flow setups: wall conditions, wall velocities, pressure forcing, steady states and the corresponding nomenclature.

Despite this growing body of work, the combined effect of wall roughness and pressure gradient altered by an abrupt changes in streamwise pressure gradient has not been systematically investigated in turbulent channel flows. In particular, the relaxation behaviour when transitioning between shear-driven and mixed pressure- and shear-driven regimes, under smooth and rough- wall conditions, remains poorly understood. In this study, we perform DNS to examine the temporal evolution of turbulent channel flows subjected to an abrupt step change in streamwise pressure gradient. Starting from statistically stationary Couette and Poiseuille–Couette base flows at $Re_\tau = 590$, we investigate both smooth–smooth and rough–smooth wall configurations.

NUMERICAL METHODOLOGY

The three-dimensional, incompressible Navier–Stokes equations are solved in non-dimensional form, using the mean channel half-height δ and the reference velocity u_{ref} (defined later) as characteristic scales. A finite-difference code is employed, operating on a staggered grid. Spatial derivatives are approximated using a second-order central difference scheme, while time advancement is performed with a second-order Adams–Bashforth method. Wall roughness is resolved using an iterative embedded-boundary algorithm described by Busse *et al.* (2015). The rough surface corresponds to a grit-blasted topography (Thakkar *et al.* 2017), with $k/\delta = 1/6$, where k is the mean peak-to-valley height. Periodic boundary conditions are imposed in the streamwise x- and spanwise y- directions. The computational domain is of size $(L_x/\delta, L_y/\delta, L_z/\delta) = (5.63, 2.815, 2.324)$ in x, y, z, with grid resolution of $(864, 432, 1024)$ points, respectively. The grid is uniform in x and y, and stretched in the wall-normal z direction. The corresponding grid spacings in wall units are $\Delta x^+ = 3.8$, $\Delta y^+ = 3.8$, while the minimum and maximum wall-normal spacings are $\Delta z^+_{\text{min}} = 0.7$ and $\Delta z^+_{\text{max}} = 2.9$, respectively. Simulations have been performed at the friction Reynolds number $Re_\tau = 590$.

Seven test cases are considered, beginning from statistically stationary states corresponding to either pure Couette flow (C) or mixed Poiseuille–Couette flow (PC). For the PC cases, the reference velocity is given by $u_{\text{ref}} = [-(\delta/\rho)(dP/dx)]^{1/2}$ such that the dimensionless pressure-gradient forcing term in the Navier-Stokes equations is given by $\Pi = -1$ and the upper (top) wall velocity is specified as $U_T = \pm 40$. The pure shear driven (C) configurations have $\Pi = 0$. For consistency with the PC cases, the same wall velocity is specified, meaning that the reference velocity for the C cases is $u_{\text{ref}} = |U_T|/40$. An abrupt change in the streamwise pressure gradient, introduced via the forcing term Π, is used to trigger the transient response. Transitions include both the onset of a pressure gradient from an initially pure shear-driven state ($\Pi = 0 \rightarrow \Pi = -1$) and the removal of pressure gradient from a mixed flow condition ($\Pi = -1 \rightarrow \Pi = 0$). In each case, two wall configurations are considered: smooth–smooth (denoted $_{SS}$) and rough-smooth (denoted $_{RS}$). The top wall moves either at a constant velocity $U_T/u_{\text{ref}} = +40$, with the superscript $^+$ indicating positive direction, or at $U_T/u_{\text{ref}} = -40$, with the superscript $^-$ indicating negative direction. Table 1 summarises the flow setups and introduces the nomenclature adopted in this study (an eighth case $APG_{SS_{01}}$ is under way).

RESULTS

Figure 1 presents steady-state velocity profiles for the Couette and mixed Poiseuille–Couette flows used as initial and final conditions. Figure 1(a) shows the mean velocity profiles in outer units. The smooth Couette case C_{SS^+} exhibits symmetry about the channel centreline ($z/\delta = 1$), while the rough-wall cases C_{RS^+} and C_{RS^-} exhibits reduced centreline velocity due to enhanced drag on the rough surface. In the mixed flow cases (PC), the imposed pressure gradient breaks the centreline symmetry. The effect of roughness is visible in PC_{RS^+}, where increased friction on the lower (rough) wall leads to further deviation from the smooth-wall profile. In contrast, reversing the wall motion in PC_{RS^-} leads to reduced friction on the rough wall, as the pressure gradient opposes the wall motion. Thus, we define the FPG side as the wall experiencing higher friction velocity, and the APG side as that with a lower friction velocity. The friction velocity at the rough wall is calculated from the balance of the x- momentum equation of a control volume, as

$$-2\frac{\delta}{\rho}\frac{dP}{dx} = u_{\tau_B}^2 \cdot \text{sign}\left(\left. \frac{d\langle\overline{u}\rangle}{dz} \right|_B \right) - u_{\tau_T}^2 \cdot \text{sign}\left(\left. \frac{d\langle\overline{u}\rangle}{dz} \right|_T \right). \quad (1)$$

where the overbar $\bar{\cdot}$ indicates a time-average and angle brackets $\langle \cdot \rangle$ the average over wall-parallel planes (*i.e.* average over x and y). u_{τ_B} and u_{τ_T} are the friction velocities on the bottom and top walls, respectively, and the signs of $d\langle\overline{u}\rangle/dz$ are inferred using the global wall-normal coordinate z. Note that, for simplicity, in the following figures, both the overbar and the angle brackets are removed, *i.e.* $\langle\overline{u}\rangle \equiv u$. In the cases where the top wall is smooth and the bottom wall is rough, the friction velocity on the rough wall can be deduced by substituting the value of the imposed pressure gradient, calculating the known u_{τ_T} on the smooth top surface by differentiation of the velocity profile, and rearranging equation 2 for the unknown u_{τ_B}.

Figure 1(b) shows the mean velocity profiles in wall units. In fully smooth-wall cases, the near-wall region exhibits the expected linear behaviour, while the presence of the adverse pressure gradient introduces a modest downward shift in the logarithmic region (see PC_{SS^-} APG). In all rough-smooth $_{RS}$ cases, roughness on the lower wall increases surface friction relative to a smooth wall, leading to a more pronounced downward shift in the log-law region. This behaviour is consistent with enhanced momentum transfer at the rough surface.

Starting from the statistically steady states described above, an abrupt change in the streamwise pressure gradient is imposed. The cases are classified as FPG or APG, according to the definitions introduced earlier. Transitions from pure Couette flow to mixed Poiseuille-Couette flow ($\Pi = 0 \rightarrow \Pi = -1$) are denoted by the subscript $_{01}$, whereas the reverse transitions ($\Pi = -1 \rightarrow \Pi = 0$) are denoted by $_{10}$ (see table 1). Figure 2 (FPG cases) and figure 3 (APG cases) show the wall-normal evolution of the mean velocity profiles at successive time intervals of $\Delta t = 10\,\delta/u_{\mathrm{ref}}$. Profiles are labelled from 10 to 50, with profile 0^+ representing the first state immediately after the abrupt change in pressure gradient. No averaging over multiple ensembles nor smoothing data technique has been used here for the transient data or in subsequent analyses. In each panel, the initial and final statistically steady profiles are also reported for reference, using the same colour code as in figure 1. The top row of each figure block (figures 2 (a-d) and 3 (a-d)) shows the velocity profiles in outer scaling. At $t = 0^+$, all profiles collapse onto the initial steady state distribution. Thereafter, all cases show a non-uniform relaxation process, with an early rapid adjustment followed by a slower evolution towards the final statistically steady state. The rough wall cases adjust more rapidly overall, reaching the final state over a shorter time interval. This two-stage adjustment aligns with the relaxation model proposed by Chung (2005) for step-change transients. However, the significantly shorter interval required for the rough-wall cases to reach equilibrium suggests that roughness accelerates the second stage of this process.

The bottom row of each block (figures 2(e-h) and 3(e-h)) shows the same data in wall units. During the transient, however, the streamwise momentum balance is no longer in a statistically steady state. Consequently, when estimating the skin friction at the bottom wall, equation 2 must include the unsteady term, which accounts for the bulk acceleration or deceleration of the flow. The appropriate integral x- momentum balance is

$$\frac{\partial}{\partial t}\int_0^{2\delta}\langle\overline{u}\rangle(z,t)\,\mathrm{d}z - 2\frac{\delta}{\rho}\frac{dP}{dx} = u_{\tau_B}^2\,\mathrm{sign}\left(\left.\frac{d\langle\overline{u}\rangle}{dz}\right|_B\right) - u_{\tau_T}^2\,\mathrm{sign}\left(\left.\frac{d\langle\overline{u}\rangle}{dz}\right|_T\right). \tag{2}$$

where the unsteady term is evaluated from the time series of the bulk transport quantity $T_x(t_k) = \frac{1}{2\delta}\int_0^{2\delta}\langle\overline{u}\rangle(z,t_k)\,\mathrm{d}z$. The spatial integral is evaluated at each saved instant t_k using the trapezoidal rule in z, while the time derivative is obtained using forward difference for snapshots $k = 1..N-1$ and backward difference for the last snapshot.

Including the unsteady term restores an exact balance in the near-wall region for all flow configurations, as confirmed by the complete overlap of the profiles at all successive time instants in this region, and in agreement with the inner-layer quasi-equilibrium state suggested by Scotti and Piomelli (2001) and Kharghani and PasandidehFard (2022). Differences emerge beyond the viscous sublayer, where the logarithmic region displays distinct relaxation behaviour. To highlight this, each figure includes an inset restricted to the log-law region. Results indicate that, while the near-wall balance adjusts in a nearly universal manner, the logarithmic layer retains a more explicit signature of the preceding equilibrium and of the direction of the forcing change. In the smooth-wall cases, the transient response appears history-dependent: depending on the direction of the forcing transition ($\Pi = 0 \rightarrow \Pi = -1$ and vice versa), the profiles may remain organised around either the initial or the final equilibrium state. This asymmetry is most evident under favourable pressure gradient conditions. For $FPG_{SS_{01}}$, the profiles are distributed around the final equilibrium, indicating a comparatively rapid reorganisation of the logarithmic layer towards the new state. By contrast, for $FPG_{SS_{10}}$, the profiles remain centred around the initial mixed Poiseuille-Couette state, showing that the logarithmic region retains memory of the pre-transition organisation. The observed directional asymmetry in the smooth-wall log layer is consistent with the different turbulence responses reported by Seddighi *et al.* (2011b) for ramp-up and ramp-down transients. Under adverse pressure gradient conditions, the smooth-wall response is more dispersed: in $APG_{SS_{10}}$, the profiles are spread around the final state, which itself remains close to the initial one, so that the transient behaviour is characterised by a broader non-equilibrium distribution about neighbouring equilibria.

A different behaviour is observed when the bottom wall is rough. In all rough-wall cases, the transient log-layer profiles evolve from the initial towards the final equilibrium, suggesting that roughness reduces the persistence of the previous state and promotes a more direct reorganisation of the overlap-layer momentum balance. Under FPG, both $FPG_{RS_{01}}$ and $FPG_{RS_{10}}$ exhibit a direct progression from the initial to the final state, with the final equilibrium reached over fewer intermediate states in both directions. Under APG, the same tendency is preserved, although the relaxation becomes less uniform. In $APG_{RS_{01}}$, the profiles evolve towards the final equilibrium but spread around it during the late stages of the adjustment, whereas in $APG_{RS_{10}}$ the transition from the initial to the final state is smooth. This result aligns with the work of Seddighi *et al.* (2011), confirming that roughness promotes a more immediate coupling between the forcing change and the structural response of the turbulence. Taken together, these results suggest that the logarithmic layer is more history-dependent for smooth walls, whereas roughness suppresses much of this memory behaviour and leads to a more direct transient adjustment towards the final equilibrium, even when the APG cases remain more irregular. Moreover, although the near-wall response is largely unaffected by the sign of the forcing change once the unsteady term is included, the logarithmic region responds differently under favourable and adverse pressure gradients. The FPG cases display a more monotonic relaxation towards the new equilibrium, whereas the APG cases remain more scattered, indicating a more persistent non-equilibrium state and a memory of the preceding flow organisation. These results resemble the structural mechanisms identified by Kharghani and PasandidehFard (2022), where favorable gradients suppress wall-normal fluctuations to create a more ordered, streamwise-dominant state, while adverse gradients enhance turbulent mixing and dispersion, thereby prolonging the non-equilibrium adjustment.

To complement the spatial (wall-normal) evolution analysis, an attempt was made to quantify the relaxation time associated with the transient response of both the inner and the bulk region of the flow by analysing the temporal evolution of representative observables $y(t)$, taken here as either the bottom-wall shear stress $\tau_{w_B}(t)/(\rho u_{\mathrm{ref}}^2)$ or, for the outer-flow response, the velocity at the inflection point $u_{\mathrm{i}}(t)/u_{\mathrm{ref}}$. For each case, the (raw) time history of the signal was first considered, and the same quantity was then normalised using the corresponding initial and final statistically steady values, y_0 and y_∞, according to $y_n(t) = [y(t) - y_\infty]/[y_0 - y_\infty]$. This normalisation maps the transient evolution onto a decay from unity to zero and facilitates comparison between cases with different absolute amplitudes. Figures 4 and 5 show the time histories of the velocity at the inflection point $u_{\mathrm{i}}(t)/u_{\mathrm{ref}}$ and of the shear stress at the bottom wall $\tau_{w_B}(t)/(\rho u_{\mathrm{ref}}^2)$, respectively, together with the corresponding normalised signals. In each panel, a single global exponential fitting curve is superposed to show the overall trend of the transient. The transient response of the outer region, represented in figure 4, appears comparatively regular. In both FPG and APG conditions, the normalised signals decay monotonically and remain close to a straight line in semilogarithmic form over a substantial portion of the evolution, indicating that the bulk adjustment is reasonably well described by a single dominant trend. A clear distinction nevertheless emerges between smooth- and rough-wall cases. Under FPG (see first column), the two smooth-wall transients display very similar rates of adjustment despite the opposite direction of the forcing change, whereas the rough-wall cases evolve more rapidly towards the final state in both directions. The same tendency is preserved under APG (see second column), where the rough-wall cases again approach the new equilibrium more quickly than the smooth-wall case, with only limited sensitivity to the direction of the transition. These observations suggest that the transient response of the outer region is primarily controlled by wall condition, with roughness promoting a faster and more direct reorganisation of the mean profile.

The time history of the shear stress is presented in figure 5. In general, it is more irregular and exhibits a stronger case-to-case dependence. Under FPG (see first column), all cases evolve monotonically towards the final state, but the normalised representation reveals a more variable degree of alignment with the global exponential guide than for the velocity at the inflection point (compare with figure 4(c)). In particular, the smooth-wall transition $FPG_{SS_{01}}$ shows a more evident curvature, suggesting a less regular adjustment, whereas $FPG_{SS_{10}}$ follows a more nearly single-stage decay. The rough-wall FPG cases reach the final state more directly, although $FPG_{RS_{01}}$ remains more dispersed than $FPG_{RS_{10}}$. Under APG (see second column), the shear stress response is again monotonic, but the dependence on the direction of the forcing change becomes more pronounced than in the outer-region signal: $APG_{RS_{01}}$ adjusts more rapidly, whereas $APG_{RS_{10}}$ and $APG_{SS_{10}}$ display a slower evolution. The comparison between $u_{\mathrm{i}}(t)/u_{\mathrm{ref}}$ and $\tau_{w_B}(t)/(\rho u_{\mathrm{ref}}^2)$ suggests that the outer-region response is comparatively regular and only weakly dependent on the direction of the transition, while the shear stress signal retains a stronger sensitivity to the forcing history and exhibits a less universal transient behaviour. Overall, the wall-normal profiles reveal how the flow reorganises in space, particularly in the logarithmic layer where history effects remain most evident, whereas the scalar signals $u_{\mathrm{i}}(t)/u_{\mathrm{ref}}$ and $\tau_{w_B}(t)/(\rho u_{\mathrm{ref}}^2)$ provide a more compact indication of the rate of adjustment. Thus, both diagnostics support the same general picture: roughness promotes a faster and more direct relaxation towards the final state, the near-wall region adjusts in a more universal manner once the unsteady term is accounted for, and the memory of the previous equilibrium is retained in the logarithmic region, especially over smooth walls.

CONCLUSIONS

DNS were conducted to investigate the transient response of turbulent channel flow to an abrupt change in the imposed streamwise pressure gradient, considering both smooth-smooth and rough-smooth wall configurations at $Re_\tau = 590$. The analysis focused on transitions between pure Couette flow and mixed Poiseuille-Couette flow and vice versa, under both favourable and adverse pressure gradient conditions, with the aim of assessing how roughness and pressure forcing/removal influence the adjustment towards a new statistically steady state. Results show that all cases undergo a non-uniform relaxation process, characterised by an initial rapid departure from the original equilibrium followed by a slower evolution towards the final state. The rough-wall cases adjust more rapidly, reaching the new equilibrium over a shorter time interval than the corresponding smooth-wall cases. Once the unsteady term is taken into account, the near-wall balance is restored for all flow configurations, indicating that the inner-layer response remains comparatively universal despite the abrupt change in forcing. Clear differences emerge farther from the wall. The wall-normal profile evolution shows that the logarithmic region retains memory of the preceding equilibrium and responds differently depending on both wall condition and pressure gradient condition. Under favourable pressure gradient conditions, the transient behaviour is monotonic, but the smooth-wall cases display a directional asymmetry. Under adverse pressure gradient conditions, the response becomes scattered, so that the departure from equilibrium is spread over a broader range of intermediate states. Within this framework, roughness plays a systematic role. In both FPG and APG cases, the rough-wall configurations evolve more directly from the initial towards the final equilibrium and reach the new state over a shorter time interval than the corresponding smooth-wall cases. Time histories of the velocity at the inflection point and of the shear stress at the bottom wall support this interpretation. As well as completing the $APG_{SS_{01}}$ case, the present findings suggest several directions for future work, including the use of ensemble averaging to obtain a more robust characterisation of the relaxation processes and the extension to intermediate conditions of both FPG and APG.

Acknowledgement: This work was supported by UKRI under EPSRC grant EP/W026090/1.

REFERENCES

Busse A., Lützner M., Sandham N.D. (2015), Direct numerical simulation of turbulent flow over a rough surface based on a surface scan. *Comput Fluids*, Vol.147, pp. 116-129.

Chung, Y. M.(2005), Unsteady Turbulent Flow with Sudden Pressure Gradient Changes, *International Journal for Numerical Methods in Fluids*, Vol. 47, pp. 925–30.

He, S. and Seddighi, M., (2013), Turbulence in Transient Channel Flow, *Journal of Fluid Mechanics*, Vol. 715, pp. 60–102.

Kharghani, M. and PasandidehFard, M. (2022), Turbulence Structures in Accelerated Flow over a Flat Plate with Non-Zero Pressure Gradient, *Journal of Applied Fluid Mechanics*, Vol. 15, pp. 311–24.

Scotti, A. and Piomelli, U., (2001), Numerical Simulation of Pulsating Turbulent Channel Flow, *Physics of Fluids*, Vol. 13, pp. 1367–84.

Seddighi, M., He, S., Orlandi, P. and Vardy, A. E. (2011b), A Comparative Study of Turbulence in Ramp-Up and Ramp-Down Unsteady Flows, *Flow, Turbulence and Combustion*, Vol. 86, pp. 439–54.

Seddighi, M., He, S., Pokrajac, D., O'Donoghue, T. and Vardy, A. E., (2015), Turbulence in a Transient Channel Flow with a Wall of Pyramid Roughness, *Journal of Fluid Mechanics*, Vol. 781, pp. 226–60.

Seddighi, M., He, S., Vardy, A. E. and Orlandi, P. (2011a), Influence of a K-Type Roughness on the Behaviour of Turbulence in an Unsteady Channel Flow, *Journal of Physics: Conference Series*, Vol. 318, p. 022021.

Thakkar, M., Busse, A. and Sandham, N. D. (2017), Surface Correlations of Hydrodynamic Drag for Transitionally Rough Engineering Surfaces. *Journal of Turbulence*, Vol. 18, pp. 138–69.

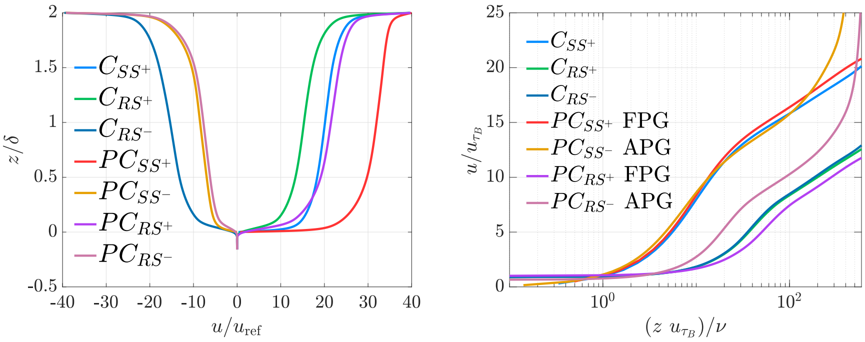

(a) (b)

Figure 1: Mean velocity profiles in outer units normalised using $u_{\rm ref}$ (a) and in wall units normalised using the friction velocity at the bottom wall u_{τ_B} (b) for all the statistically stationary states.

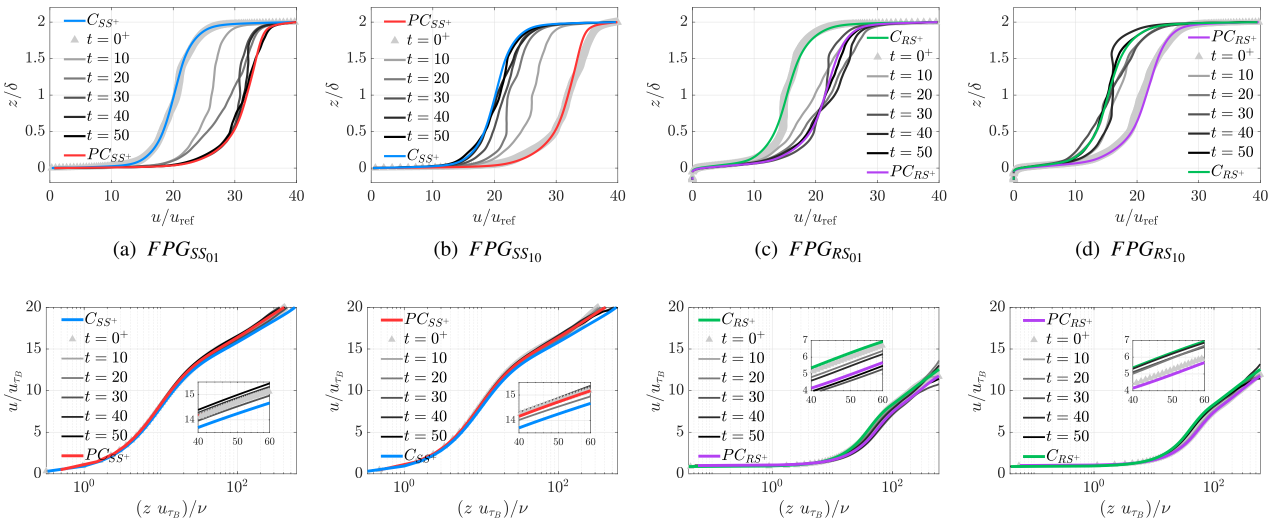

(a) $FPG_{SS_{01}}$ (b) $FPG_{SS_{10}}$ (c) $FPG_{RS_{01}}$ (d) $FPG_{RS_{10}}$

(e) $FPG_{SS_{01}}$ (f) $FPG_{SS_{10}}$ (g) $FPG_{RS_{01}}$ (h) $FPG_{RS_{10}}$

Figure 2: Evolution of the mean velocity profiles normalised using $u_{\rm ref}$ (first row) and in wall units normalised using the friction velocity at the bottom wall u_{τ_B} (second row) for the FPG cases.

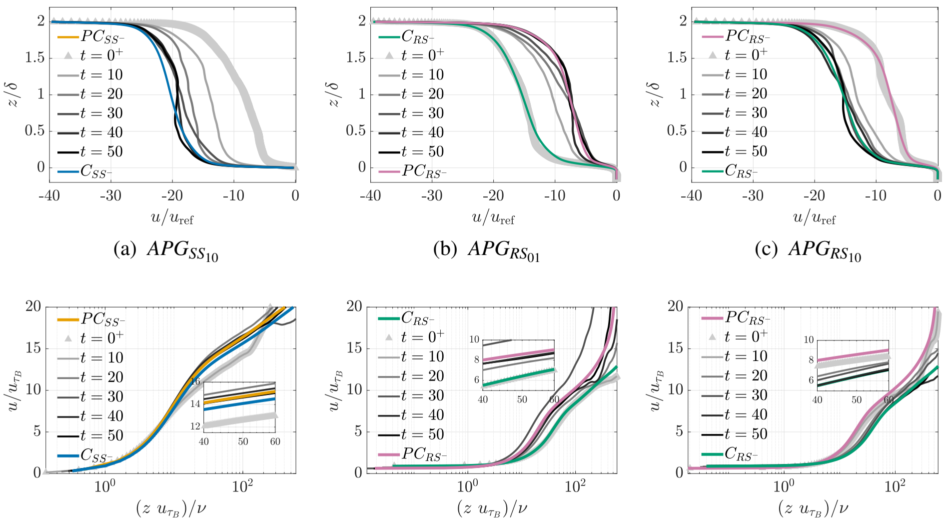

(a) $APG_{SS_{10}}$ (b) $APG_{RS_{01}}$ (c) $APG_{RS_{10}}$

(d) $APG_{SS_{10}}$ (e) $APG_{RS_{01}}$ (f) $APG_{RS_{10}}$

Figure 3: Evolution of the mean velocity profiles normalised using $u_{\rm ref}$ (first row) and in wall units normalised using the friction velocity at the bottom wall u_{τ_B} (second row) for the APG cases.

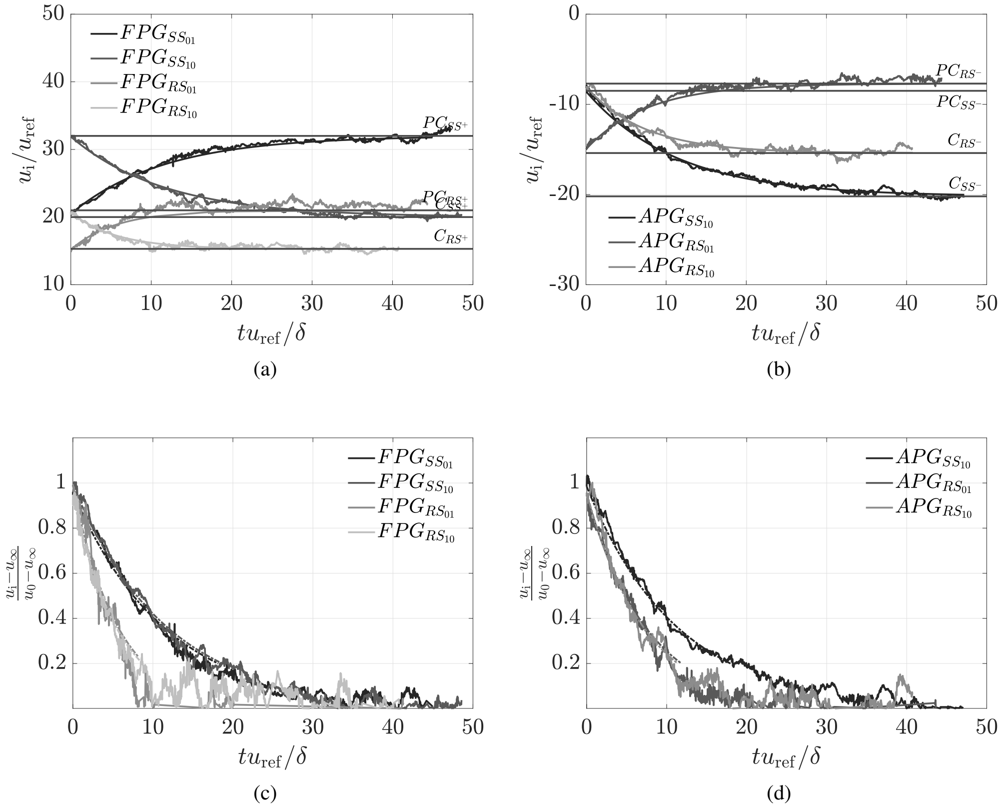

Figure 4: Time history of the velocity extracted at the inflectional point $u_i(t)/u_{ref}$ for the FPG (first column) and APG cases (second column). The corresponding normalised signals are shown below each raw time history panel.

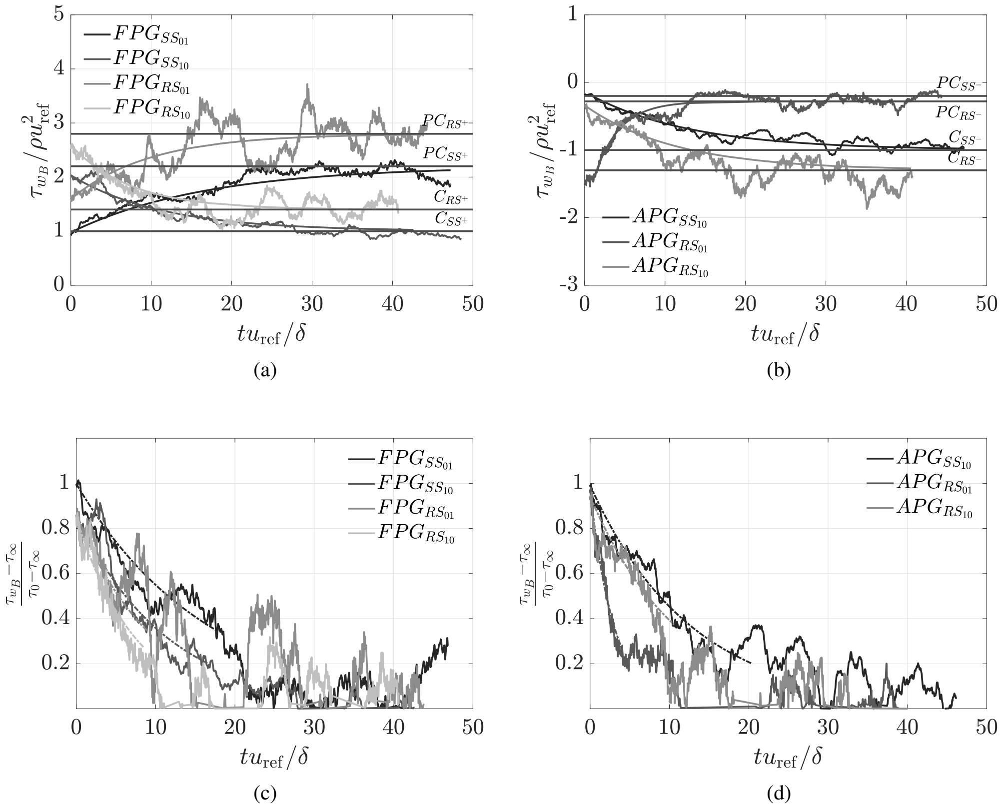

Figure 5: Time history of the shear at the bottom wall $\tau_{w_B}(t)/(\rho u_{ref}^2)$ for the FPG (first column) and APG cases (second column). The corresponding normalised signals are shown below each raw time history panel.